Understanding Impedance Ratio Criteria for Converter-Based AC Power System

Chongbin Zhao, *Student Member*, *IEEE*, and Qirong Jiang

***Abstract*—Nyquist criterion-based impedance ratio criteria (IRCs) have been widely applied for inspecting the risk of small-signal instability among converter-based AC power systems. Aided by a comparative study on voltage source converter, including the single-input single-output (SISO) and multiple input multiple output (MIMO) analyses in both the *dq* and the sequence domain, two aspects are emphasized in this paper: 1) the sufficiency of SISO analysis when the mapping function (MF) is observable to potentially unstable modes, and 2) the inconvenience of IRCs with an unintended right-half plane pole emergence of MF due to the source-load partition. The strictness of analyses is proved by a systematical deduction of explicit analytical impedance models using the state space. Moreover, a novel criterion that relies on the logarithmic derivative of MFs is proposed, which can identify the system modes directly, serve as an alternative to IRCs, and be extended to other transfer function-based stability analyses.**

***Index Terms*—Impedance model, state space, stability criterion, source-load partition, AC power systems, mapping function**

I. Introduction

IMPEDANCE ratio criteria (IRCs) for converter-based AC power systems, which were first deduced in the *dq* [1] and then extended to the sequence domain [2], is proved to be a powerful tool for analyzing the small-signal stability that can protect the privacy of vendors. A relevant standard [3] has been formed to guide the construction of wind farms in China, which confirms the practicability of IRCs in the real world.

Port impedance/admittance models (IMs/AMs) of both load and source subsystems at a single converter-grid interface are required before applying the two-dimensional (2-d) IRC and forms a multiple input multiple output (MIMO) analysis. In general, the frequency responses instead of the detailed expressions are available for the 2-d transfer function matrixes with no zero-sequence differential-mode path in the three-phase AC system. Fig.1 shows that a couple of port IM/AM can export to two decoupled one-dimensional (1-d) *loop* IMs, and two 1-d IRCs can be derived after partitioning loop IMs [4] to achieve the single input single output (SISO) analyses. Suppose that the converter operates in a current source mode, it is normally considered that as long as the converter is stable when powered by an ideal voltage source, that is, no right half plane (RHP) pole exists in the 2-d AM, the marginal stability condition of various IRCs should be the same. Such an equivalence is guaranteed by the linear frame transformation [4] and the uniformity of mapping function (MF) using Schur complement (MF maps the Nyquist contour in *s* plane to the Nyquist plots in ω plane according to Cauchy's argument principle). However, the lack of authentic zeros and poles (*Z*s and *P*s, mainly the *P*s) for MFs may cause difficulties in the practical graphical stability assessments.

The scope of this paper is to conduct a comparative study, reveal several overlooked details of IRC, and inspire future stability analysis. The order of targeted grid-connected system is quite low, thus IMs/AMs can be deduced from the state space to obtain the exact *Z*s and *P*s. Nyquist plots are checked with the *Z*s and *P*s of MFs to clarify the advantage of 1-d IRC, and it is found that the stable operation of AC subsystems does not guarantee *no* RHP pole in the loop IM. Hence, it is recommended to apply the proposed stability criterion based on the logarithmic derivative of loop IM with only frequency responses used, which is easy to implement and worthy of extending to other transfer function-based stability analyses [5].

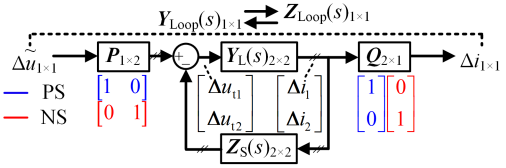

Fig. 1. A generalized representation of the closed-loop system.

II. IM/AM Derivation Using State Space

A. System Overview

Fig. 2 shows the typical grid-following control loops of a three-phase symmetrical two-level voltage source converter (VSC), which act as a current source in parallel with an output impedance in the frequency domain, i.e., the load subsystem [2]. The *d*-axis outer loop regulates the DC voltage while the reference of *q*-axis outer loop is set to 0. The use of VSC average model in the simulation avoids the complicated effects of PWM on stability analyses. Table I lists the key parameters for comparative studies.

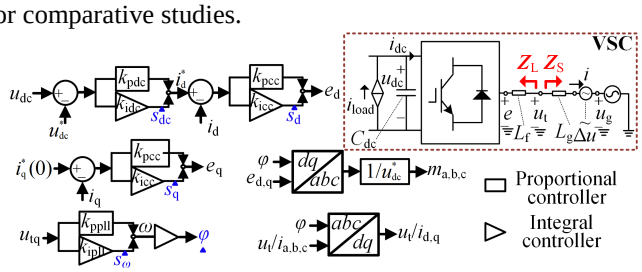

Fig. 2. Control loops of VSC. Superscript * means reference.

TABLE I
KEY PARAMETERS OF SYSTEM

This work was supported in part by the National Natural Science Foundation of China under Grant U1866601. *(Corresponding author: Qirong Jiang).*

C. Zhao and Q. Jiang are with the Department of Electrical Engineering, Tsinghua University, Beijing 100084, China (e-mail: zhaocb19@mails.tsinghua.edu.cn; qrjiang@mail.tsinghua.edu.cn).

Symbols	Case 1	Case 2
$\boldsymbol{u_g}$, $\boldsymbol{u_{dc}^*}$, $\boldsymbol{\omega_0}$	380V, 750V, 2π50rad/s	380V, 750V, 2π50rad/s
$\boldsymbol{L_f}$, $\boldsymbol{L_g}$, $\boldsymbol{C_{dc}}$	0.55mH, 0.8~1mH, 5mF	5mH, 2.1~2.3mH, 5mF
$\boldsymbol{i_{load}}$	66.66A	3.1A
$\boldsymbol{k_{pdc}}$+$\boldsymbol{k_{idc}}$/s	0.1+100/s	1+100/s
$\boldsymbol{k_{pcc}}$+$\boldsymbol{k_{icc}}$/s	0.1+10/s	1+1000/s
$\boldsymbol{k_{ppll}}$+$\boldsymbol{k_{ipll}}$/s	3+100/s	5+2000/s

B. Modeling Process

It is well-recognized that the modes of the complete system can be identified through the eigenvalue analysis, and the negative damping mode induces the oscillation. By computing the system equilibrium, regarding the small-signal of voltage/current as input/output, and adjusting the state equations, the 2×2 port AM of both VSC and grid, as well as the decoupled 1-d loop AMs, are first deduced in the *dq* domain [1], [6]. The process is described as:

$$\begin{cases}\Delta\dot{\boldsymbol{x}}_{\rm dq}=\boldsymbol{A}_{\rm dq}\Delta\boldsymbol{x}_{\rm dq}+\boldsymbol{B}_{\rm dq}\Delta\boldsymbol{u}_{\rm dq}\\ \Delta\boldsymbol{y}_{\rm dq}=\boldsymbol{C}_{\rm dq}\Delta\boldsymbol{x}_{\rm dq}+\boldsymbol{D}_{\rm dq}\Delta\boldsymbol{u}_{\rm dq}\end{cases},\Delta\boldsymbol{u}_{\rm dq}=\underbrace{[\boldsymbol{C}_{\rm dq}(s\boldsymbol{I}-\boldsymbol{A}_{\rm dq})^{-1}\boldsymbol{B}_{\rm dq}+\boldsymbol{D}_{\rm dq}]}_{\boldsymbol{Y}_{\rm dq}}\Delta\boldsymbol{y}_{\rm dq},\boldsymbol{Z}_{\rm dq}=\boldsymbol{Y}_{\rm dq}^{-1}. \tag{1}$$

where $\boldsymbol{A}$, $\boldsymbol{B}$, $\boldsymbol{C}$, and $\boldsymbol{D}$ are Jacobian matrixes; $\boldsymbol{x}$, $\boldsymbol{y}$, and $\boldsymbol{u}$ are state, output, and input vectors formed by the 8 variables in Fig. 2, including 3 of energy storage device and 5 of integrator output, and the variables are distinguished by whether appear in *dq* pairs (e.g. [$s_{\rm d}$, $s_{\rm q}$]). The prefix Δ and the subscript dq represent the small signals and *the system dq axis* [7]; Y and Z represent AMs and YMs, while s represent the imaginary unit.

Realizing there is a combination of rotation and complex transformation from a *dq* domain real vector to a sequence domain complex vector (with the subscript dq and pn respectively) [7] in (2), (1) is transformed to (3):

$$\boldsymbol{A}_{\rm pn}=\boldsymbol{T}_{\rm x}^{-1}(\boldsymbol{A}_{\rm dq}+{\rm j}\omega_0\boldsymbol{I})\boldsymbol{T}_{\rm x},\boldsymbol{B}_{\rm pn}=\boldsymbol{T}_{\rm x}^{-1}\boldsymbol{B}_{\rm dq}\boldsymbol{T}_{\rm u},\boldsymbol{C}_{\rm pn}=\boldsymbol{T}_{\rm y}^{-1}\boldsymbol{C}_{\rm dq}\boldsymbol{T}_{\rm x},\boldsymbol{D}_{\rm pn}=\boldsymbol{T}_{\rm y}^{-1}\boldsymbol{D}_{\rm dq}\boldsymbol{T}_{\rm u}. \tag{2}$$

$$\begin{cases}\Delta\dot{\boldsymbol{x}}_{\rm pn}=\boldsymbol{A}_{\rm pn}\Delta\boldsymbol{x}_{\rm pn}+\boldsymbol{B}_{\rm pn}\Delta\boldsymbol{u}_{\rm pn}\\ \Delta\boldsymbol{y}_{\rm pn}=\boldsymbol{C}_{\rm pn}\Delta\boldsymbol{x}_{\rm pn}+\boldsymbol{D}_{\rm pn}\Delta\boldsymbol{u}_{\rm pn}\end{cases},\Delta\boldsymbol{u}_{\rm pn}=\underbrace{[\boldsymbol{C}_{\rm pn}(s\boldsymbol{I}-\boldsymbol{A}_{\rm pn})^{-1}\boldsymbol{B}_{\rm pn}+\boldsymbol{D}_{\rm pn}]}_{\boldsymbol{Y}_{\rm pn}}\Delta\boldsymbol{y}_{\rm pn},\boldsymbol{Z}_{\rm pn}=\boldsymbol{Y}_{\rm pn}^{-1}. \tag{3}$$

In (2), the item j$\omega_0\boldsymbol{I}$ reflects the rotation, where j is the imaginary unit, ω_0 is the rated angular frequency, and $\boldsymbol{I}$ is the utility matrix. $\boldsymbol{T}$ represents the complex transformation, whose order is determined by the vector of subscript, where the submatrix 0.5×[1, 1; –j, j] cooperates with the *dq* pairs [7].

Compared with IM/AM derived by frequency domain linearization and intermediate variables elimination, the distinct advantage of the proposed modeling process is that it can ensure the number of AM poles equals that of state variables, which helps observe the real case of zero-pole cancellation and avoids the dimension explosion of IM/AM.

Applying the 1-d IRC requires a reconstruction of source-load IM from the 2-d port IMs obtained by (1) and (3) [4]:

$$\boldsymbol{Z}_{\rm L/S}^{1}=\boldsymbol{Z}_{\rm L/S}^{11}-\frac{\boldsymbol{Z}_{\rm L/S}^{12}(\boldsymbol{Z}_{\rm L/S}^{21}+\boldsymbol{Z}_{\rm S/L}^{21})}{\boldsymbol{Z}_{\rm L/S}^{22}+\boldsymbol{Z}_{\rm S/L}^{22}},\boldsymbol{Z}_{\rm L/S}^{2}=\boldsymbol{Z}_{\rm L/S}^{22}-\frac{\boldsymbol{Z}_{\rm L/S}^{21}(\boldsymbol{Z}_{\rm L/S}^{12}+\boldsymbol{Z}_{\rm S/L}^{12})}{\boldsymbol{Z}_{\rm L/S}^{11}+\boldsymbol{Z}_{\rm S/L}^{11}} \tag{4}$$

where the subscript L/S represents the load/source subsystem, the superscript of a two-digit number indicates the coordinate of element in the 2-d port IM, while the superscript of a one-digit number indicates the order of obtained equivalent 1-d port IM in (4). It can be verified that the sum of $\boldsymbol{Z}_{\rm L}^{1/2}$ and $\boldsymbol{Z}_{\rm S}^{1/2}$ is equal to the 1-d loop IM deduced from (1) and (3), hence (4) is also a source-load partition of the 1-d loop IM regardless of modeling in the *dq* and the sequence domain.

III. Stability Analysis Using IRCs

A. Simulation Results

For both cases in Table I, VSC is ensured to be in stable operation when powered by the ideal voltage source (the phase and amplitude of the voltage source are determined by the power flow with various grid inductors $L_{\rm g}$s), and IRCs are allowed to use from the conventional perspective [2]. Taking the condition of $L_{\rm g}$=max($L_{\rm g}$) as an example, by calculating the eigenvalues of $\boldsymbol{A}_{\rm dq}$, Table II shows that no RHP pole exists in each element of port AM, which is a *necessary and sufficient condition* for the independent stable operations of subsystems.

TABLE II
Poles of dq Domain AMs (×10²)

Case 1	–1.32±j4.53	–0.40±j0.75	–0.09±j0.49	–8.91	–0.35
Case 2	–7.67±j1.60	–1.13±j6.31	–0.26±j3.24	–0.62±j0.86	

The time-domain simulation is then performed in PSCAD to serve as a standard for theoretical analyses. Fig. 3 shows the waveform of DC voltage $u_{\rm dc}$ in case 1. The system becomes unstable if the grid $L_{\rm g}$ steps from 0.9 mH to 1 mH, and a similar phenomenon happens when $L_{\rm g}$ steps from 2.2 mH to 2.3 mH in case 2 (the waveform is neglected for brevity). Such phenomena conform to a general cognition that the system tends to be unstable due to the interaction between the phase-locked loop and weak grid, and can be analyzed using IRCs at the AC converter-grid interface since the MFs discussed below are observable to the unstable mode [5].

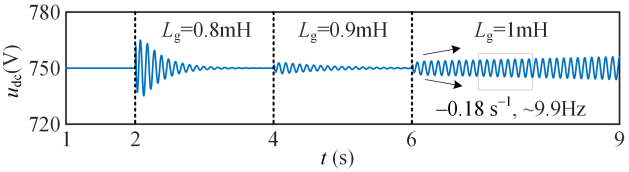

Fig. 3. Simulation waveforms of case 1.

B. Study on Case 1

Since the case-by-case simulation is time-consuming, a high-fidelity theoretical analysis is of practical requirements, and it is significant to deepen the understanding of mainstream IRCs. Nyquist plots in Fig. 4 and 5 are obtained by first calculating the matrix division of frequency response of source to load subsystems, and then calculate the eigenvalues of the matrix quotients. The legends of *d*, *q*, *p*, and *n* below represent the trajectories of each domain in 1-d IRCs with explicit physical meaning, while the legends of eig 1&2 represent the trajectories of eigenvalues in 2-d IRCs.

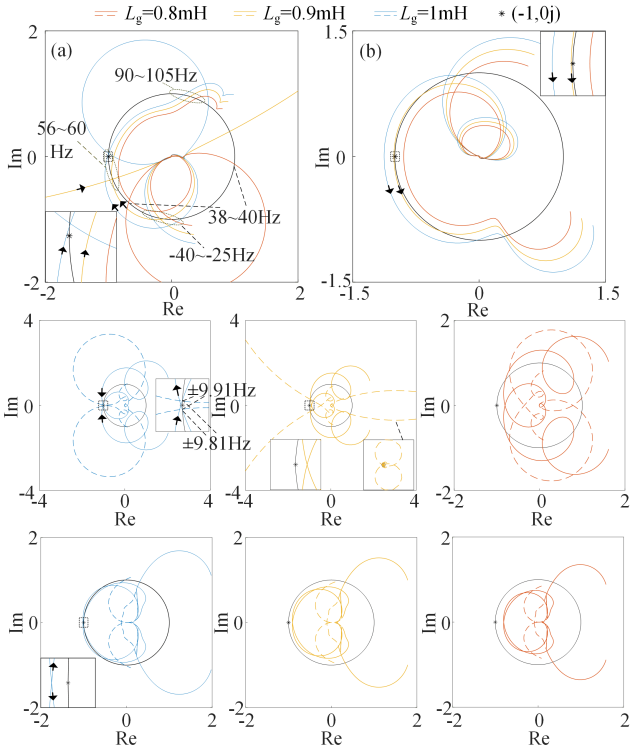

Fig. 4. Nyquist plots of case 1. (a) 1-d (sequence, p). (b) 2-d (sequence, eig 1). (c) 1-d (*dq*, *d*&*q*). (d) 2-d (*dq*, eig 1&2).

TABLE III
*Z*s-*P*s OF MF_as ($\times 10^2$, Case 1)

	Z	***d*, *q***	**0.0018±j0.62**	–0.61±j4.07	–0.27±j0.48	–0.35	–2.26
	P	***d***	–1.02±j4.72	–0.38±j0.93	–0.10±j0.49	–0.35	–2.19
		q	–0.94±j3.77	–0.30±j0.44	**0.10±j0.58**	–0.35	–8.91
L_g= 1m H	***Z***	***p*, *n***	**0.0018+j3.76**	–0.61+j7.21	–0.27+j3.62	–0.35+j3.14	–2.26+j3.14
			0.0018+j2.52	–0.61–j0.93	–0.27+j2.67		
	P	***p***	–5.29+j3.12	–0.55+j7.18	–1.72–j1.02	–0.41+j3.76	
			–0.068+j3.63	–0.35+j3.13	–0.28+j2.67	**0.024+j2.48**	
		n	–5.29+j3.17	–0.55–j0.90	–1.72+j7.31	–0.41+j2.52	
			–0.068+j2.65	–0.35+j3.15	–0.28+j3.61	**0.024+j3.80**	
	Z	***d*, *q***	–0.015±j0.62	–0.66±j4.10	–0.27±j0.49	–0.35	–2.46
	P	***d***	–1.05±j4.73	–0.40±j0.91	–0.10±j0.49	–0.35	–2.41
		q	–0.95±j3.81	–0.30±j0.45	0.002±j0.58	–0.35	–8.92
L_g= 0.9 m H	***Z***	***p*, *n***	–0.015+j3.76	–0.66–j0.96	–0.27+j3.63	–0.35+j3.14	–2.46+j3.14
			–0.015+j2.52	–0.66+j7.24	–0.27+j2.65		
	P	***p***	–5.43+j3.10	–0.58+j7.22	–1.69–j1.03	–0.41+j3.77	
			–0.068+j3.63	–0.35+j3.13	–0.27+j2.66	**0.0020+j2.48**	
		n	–5.43+j3.19	–0.58–j0.94	–1.69+j7.32	–0.41+j2.51	
			–0.068+j2.65	–0.35+j3.15	–0.27+j3.62	**0.0020+j3.80**	
	Z	***d*, *q***	–0.033±j0.62	–0.71±j4.13	–0.27±j0.51	–0.35	–2.70
	P	***d***	–1.05±j4.73	–0.40±j0.91	–0.10±j0.49	–0.35	–2.41
		q	–0.95±j3.81	–0.30±j0.45	0.002±j0.58	–0.35	–8.92
L_g= 0.8 m H	***Z***	***p*, *n***	–0.033+j3.76	–0.71+j7.26	–0.27+j2.64	–0.35+j3.14	–2.70+j3.14
			–0.033+j2.53	–0.71–j0.98	–0.27+j3.65		
	P	***p***	–5.60+j3.10	–0.62+j7.26	–1.65–j1.05	–0.41+j3.78	
			–0.071+j3.63	–0.35+j3.13	–0.26+j2.64	–0.022+j2.48	
		n	–5.60+j3.20	–0.58–j0.98	–1.69+j7.33	–0.41+j2.50	
			–0.071+j2.65	–0.35+j3.15	–0.26+j3.65	–0.022+j3.80	

Fig. 4 illustrates the Nyquist plots of case 1. To improve the persuasiveness of graphical stability assessments, the *Z*s and *P*s of the decoupled *type-a* MFs, i.e., MF_as, are calculated and shown in Table III, and MF_a is defined as:

$$\begin{aligned} MF_a(s) &= 1+\boldsymbol{Z}_S^{1/2}/\boldsymbol{Z}_L^{1/2} = 1+[n_S(s)/d_S(s)]/[n_L(s)/d_L(s)] \\ &= [d_S(s)n_L(s)+d_L(s)n_S(s)]/[d_S(s)n_L(s)], 1\equiv d \text{ or } p, 2\equiv q \text{ or } n. \end{aligned} \quad (5)$$

The *numerator* of MF_a is the closed-loop characteristic polynomial of the system, whose roots are equal to the system eigenvalues. Please note that MF_a is preferred for 1-d IM, since establishing the Smith-Macmillan form of transfer functions matrixes is complicated, and due to the dimension explosion, even if using the MATLAB function *mineral*, it is unlikely to obtain the accurate zeros whose number should be equal to that state variables. Because of the nonzero non-diagonal elements of the source subsystem (i.e., the grid) port IM, *minreal* is unavoidable when calculating the *Z*s and *P*s of the *dq* domain in Table III, and determining the tolerance of *Z*-*P* cancellation is a matter of trial and error. Besides, it is intuitive from Table III that the conjugate symmetries exist for two MF_as mutually about $j\omega_0$ in the sequence domain while separately about 0 in the *dq* domain, and an offset $j\omega_0$ exists for the zeros between MF_as in two domains. Therefore, when the frequency range is selected as –100 to 100 Hz for the sequence domain while –50 to 150 Hz for the *dq* domain, the consistency of stability assessments in the two domains and the feasibility of omitting a trajectory of the sequence domain in Fig. 4 and 5 are ensured.

With the bold RHP *Z*s and *P*s in Table III and the arrows to show the directions of (–1, 0j) encirclement, the particularity of case 1 is analyzed as below:

1) For the sequence domain analysis, Fig. 4 (a) of 1-d IRC shows that there is one clockwise encirclement when L_g=1mH but one counterclockwise encirclement when L_g=0.9mH, both of (–1, 0j). One can conclude that the system is unstable when L_g=1mH but cannot conclude that the system is stable when L_g=0.9mH except by inspecting the RHP poles of MF_a (or the open loop gain MF_a–1, the results are the same), and an RHP pole emerges for the 1-d loop IM when L_g=1&0.9mH even if both subsystems can stable operate separately. Furthermore, if one avoids the 1-d IRC but focuses on the 2-d IRC, it is more confusing that the feature of trajectory does not change when L_g decreases from 1mH to 0.9mH in Fig. 4 (b). Here the instability when L_g=1mH cannot even be ascertained since the trajectory encircles (–1, 0j) counterclockwise and the poles are unavailable.
2) For the *dq* domain analysis, Fig. 4 (c) of 1-d IRC shows that when L_g=1mH, there are two clockwise encirclements of (–1, 0j) for the *d*-trajectory instead of the *q*-trajectory. One may infer that the *d*-axis control leads to the instability, but it is not rigorous since *q*-MF_a owns two *Z*s and two *P*s, and the no encirclement can also judge the system unstable, which is unusual for using IRC and further indicates the significance of acquiring RHP poles of MFs. Combining 1), the consistency of stability assessment using 1-d IRCs in two domains is proved by only a frequency shift of *Z*s in Table III. The rule of rest trajectories in Fig. 4 (c) and 4 (d) satisfies the general cognition of IRCs, which is related to a much simpler *Z*-*P* distribution in Table III.
3) The preference of selecting a certain intersection point between the trajectory and unit cycle as the unstable mode

does not work in case 1, especially for the sequence domain analysis in Fig.4 (a), since none of the frequency of intersection points corresponds to the simulated (50±9.9) Hz, and the phase margin derived by various IRCs are not consistent obviously. Such a risk on the system mode identification error should be realized in the frequency domain analyses, since IRCs can only judge whether or not the system is stable with no more accurate quantitative information offered theoretically.

C. Study on Case 2

To realize that the findings of case 1 are not general, case 2 is well-studied with a similar process to case 1. On the whole, it is intuitive for each type of IRC to judge the stability through Fig. 5 with the simpler *Z-P* distribution in Table IV, except the 2-d IRC in Fig. 5 (a) since the counterclockwise encirclement of (–1, 0j) can be observed, but the feature of trajectory changes when L_g decreases from 2.3mH to 2.2mH, which differs from Fig. 4 (b), and case 2 is similar with the usage of IRCs in [4] but cannot cover the special case 1. That is to say, only if the stable closed-loop system with no RHP pole can ensure the creditable graphical stability assessments as [2] pointed out.

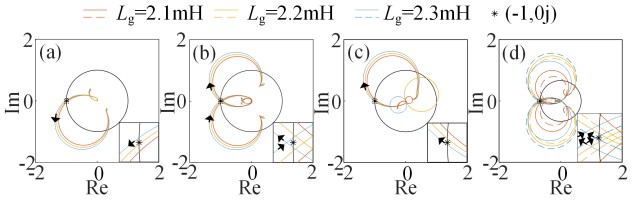

Fig. 5. Nyquist plots of case 2. (a) 2-d (sequence, eig 1). (b) 2-d (*dq*, eig 1&2). (c) 1-d (sequence, p). (d) 1-d (*dq*, *d*&*q*).

TABLE IV
*Z*s-*P*s OF MF$_a$s (×10^2, Case 2)

L_g=2.3 mH	*Z*	*d*, *q*	**0.0033±j2.94**	–0.63±j0.84	–0.79±j6.18	–5.24±j3.35
	P	*d*	–0.90±j6.48	–5.23±j3.35	–0.22±j3.35	–0.62±j0.86
		q	–7.67±j1.60	–1.04±j5.96	–0.030±j2.89	–0.63±j0.84
	Z	*p*, *n*	**0.0033+j6.08**	–0.63+j3.98	–0.79+j9.32	–5.24+j6.49
			0.0033+j0.20	–0.63+j2.30	–0.79–j3.03	–5.24–j0.20
	P	*p*	–0.80+j9.15	–6.46+j6.04	–6.36+j0.10	–1.21–j3.17
			–0.26+j6.39	–0.60+j4.01	–0.65+j2.31	**0.0065+j0.20**
		n	–0.80–j2.87	–6.46+j0.24	–6.36+j6.18	–1.21–j9.45
			–0.26–j0.10	–0.60+j2.28	–0.65+j3.98	**0.0065+j6.08**
L_g=2.2 mH	*Z*	*d*, *q*	–0.0056±j2.94	–0.63±j0.84	–0.80±j6.18	–5.31±j3.33
	P	*d*	–0.91±j6.48	–5.30±j3.33	–0.22±j3.33	–0.62±j0.86
		q	–7.67±j1.59	–1.04±j5.97	–0.037±j2.90	–0.63±j0.84
	Z	*p*, *n*	–0.0056+j6.10	–0.63+j3.98	–0.80+j9.32	–5.31+j6.48
			–0.0056+j0.19	–0.63+j2.30	–0.80–j3.04	–5.31–j0.19
	P	*p*	–0.81+j9.16	–6.50+j6.02	–6.40+j0.13	–1.21–j3.17
			–0.26+j6.39	–0.60+j4.01	–0.64+j2.30	–0.0028+j0.19
		n	–0.81–j2.88	–6.50+j0.26	–6.40+j6.15	–1.21+j9.45
			–0.26–j0.10	–0.60+j2.28	–0.64+j3.98	–0.0028+j6.10
L_g=2.1 mH	*Z*	*d*, *q*	–0.015±j2.97	–0.63±j0.84	–0.82±j6.18	–5.38±j3.32
	P	*d*	–0.92±j6.48	–5.38±j3.33	–0.22±j3.33	–0.62±j0.86
		q	–7.67±j1.58	–1.04±j5.98	–0.045±j2.92	–0.63±j0.84
	Z	*p*, *n*	–0.015+j6.11	–0.63+j3.98	–0.82+j9.32	–5.38±j6.46
			–0.015+j0.17	–0.63+j2.30	–0.82–j3.04	–5.38–j0.17
	P	*p*	–0.82+j9.18	–6.54+j6.00	–6.45+j0.16	–1.20–j3.17
			–0.26+j6.39	–0.60+j4.01	–0.64+j2.30	–0.01+j0.17
		n	–0.82–j2.89	–6.54+j0.29	–6.45+j6.12	–1.20+j9.45
			–0.26–j0.10	–0.60+j2.28	–0.64+j3.98	–0.01+j6.11

D. Summary

From the comparative study, even if 1-d IRCs of both domains correctly judge the stability, the unintended RHP poles of MF due to the source-load partition result in inconvenience for using IRCs, because the analyses will rely on accurate *Z-P* calculation and is not practical in application, which promotes a novel criterion using the frequency response of MF.

IV. Loop IM-Based Stability Criterion

A. Basic Principle

The loop IM and be selected as another MF and defined as the *type-b*, i.e., MF$_b$, since MF$_a$ and MF$_b$ hold the same closed-loop characteristic polynomial:

$$\begin{aligned}\mathrm{MF_b}(s) &= \boldsymbol{Z}_S^{1/2} + \boldsymbol{Z}_L^{1/2} = n_S(s)/d_S(s) + n_L(s)/d_L(s) \\ &= [d_S(s)n_L(s) + d_L(s)n_S(s)]/[d_S(s)d_L(s)], 1 \equiv d \text{ or } p, 2 \equiv q \text{ or } n.\end{aligned} \tag{6}$$

Rewriting MF$_b$ in a factored *Z-P* form gives:

$$\mathrm{MF_b}(s) = \prod_{i=1}^{8} a_{Zi}(s - Z_i) \Big/ \prod_{i=1}^{8} a_{Pi}(s - P_i), s = \mathrm{j}\omega. \tag{7}$$

where *a* is the flat gain. Since the essential scope of stability analysis is to identify a positive real part of Z_i, the basic unit of MF$_b$, a first-order polynomial $g_Z(\omega)=a_Z(\mathrm{j}\omega-\lambda_Z)$, $\lambda_Z=\alpha_Z+\mathrm{j}\omega_Z$, is focused. Recalling that the criterion in [6] regards the rest of MF$_b$ as a whole, requires complex square root operations and irrational approximations, the *logarithmic derivative* acts on g_Z is to eliminate the effect of a_Z and equalize each basic unit:

$$\begin{aligned}D_L(g_Z) &= d\log(g_Z)/d\omega = d(g_Z)/(g_Z d\omega) \\ &= \mathrm{j}/(\mathrm{j}\omega - \lambda_Z) = \mathrm{j}/[-\alpha_Z + \mathrm{j}(\omega - \omega_Z)]\end{aligned} \tag{8}$$

The real-imaginary (Re-Im) separation projects a complex output of $D_L(g_Z)$ to two real outputs for quantitative analysis:

$$\begin{cases}\mathrm{Re}[D_L(g_Z)] = (\omega-\omega_Z)/[(\omega-\omega_Z)^2+\alpha_Z{}^2] \\ \mathrm{Im}[D_L(g_Z)] = -\alpha_Z/[(\omega-\omega_Z)^2+\alpha_Z{}^2]\end{cases} \\ \Rightarrow \mathrm{Re}[D_L(g_Z)]\big|_{\omega=\omega_Z} = 0, \mathrm{Im}[D_L(g_Z)]\big|_{\omega=\omega_Z} = -1/\alpha_Z. \tag{9}$$

Eq. (9) shows that at $\omega=\omega_Z$, a zero-crossing point exists for Re[$D_L(g_Z)$]. To better understand $D_L(g_Z)$ at $\omega=\omega_Z$, the first and second derivatives of Re[$D_L(g_Z)$] and Im[$D_L(g_Z)$] are deduced:

$$\begin{cases}\dfrac{d\{\mathrm{Re}[D_L(g_Z)]\}}{d\omega} = \dfrac{-(\omega-\omega_Z)^2+\alpha_Z{}^2}{[(\omega-\omega_Z)^2+\alpha_Z{}^2]^2} \\ \dfrac{d\{\mathrm{Im}[D_L(g_Z)]\}}{d\omega} = \dfrac{-2(\omega-\omega_Z)^2\alpha_Z}{[(\omega-\omega_Z)^2+\alpha_Z{}^2]^2}\end{cases} \\ \Rightarrow d\{\mathrm{Re}[D_L(g_Z)]\}/d\omega\big|_{\omega=\omega_Z} = 1/\alpha_Z{}^2, d\{\mathrm{Im}[D_L(g_Z)]\}/d\omega\big|_{\omega=\omega_Z} = 0, \\ \begin{cases}\dfrac{d^2\{\mathrm{Re}[D_L(g_Z)]\}}{d\omega^2} = \dfrac{-2(\omega-\omega_Z)[3\alpha_i{}^2-(\omega-\omega_i)^2]}{[(\omega-\omega_Z)^2+\alpha_Z{}^2]^3} \\ \dfrac{d^2\{\mathrm{Im}[D_L(g_Z)]\}}{d\omega^2} = \dfrac{-6(\omega-\omega_Z)^2\alpha_Z{}^2+2\alpha_Z{}^3}{[(\omega-\omega_Z)^2+\alpha_Z{}^2]^3}\end{cases} \\ \Rightarrow d^2\{\mathrm{Re}[D_L(g_Z)]\}/d\omega^2\big|_{\omega=\omega_Z} = 0, d^2\{\mathrm{Im}[D_L(g_Z)]\}/d\omega^2\big|_{\omega=\omega_Z} = 2/\alpha_Z{}^3. \tag{10}$$

Therefore, when $\alpha_Z>0$, a negative minimum of Im[$D_L(g_Z)$] and a positive slope of Re[$D_L(g_Z)$] coexist at $\omega=\omega_Z$, and a dual relationship satisfies for Re[$D_L(1/g_Z)$] and Im[$D_L(1/g_Z)$], where $(1/g_Z)$ can be deemed as a basic unit that contains a pole in MF$_b$. The frequency selectivity induced by the inverse square term of ω in (9) suppresses the interactions between each *Z-P*, thus the weak negative damping mode can be identified quite exactly using (9) and (10). By substituting MF$_b$ into $D_L()$, the complete

process of applying the novel stability criterion is:

1) Obtaining the frequency responses of loop IMs, by either adopting the frequency sweep in analytical expressions or employing the data-driven method for black-box VSCs [5].
2) Calculating the logarithmic derivative of frequency responses based on the first line in (8), cooperating with the *difference method* (using a small step such as 0.01Hz).
3) The system is determined as unstable when a minimum of Im[$D_L(g_Z)$] and a positive slope of Re[$D_L(g_Z)$] coexist at the same frequency ($\omega=\omega_Z$), and α_Z is identified using the output of Im{$D_L[g_Z(\omega_Z)]$} and (9).

The proposed criterion draws lessons from Section III that a 1-d MF is adequate to judge the stability. It avoids the influence of *P*s on the stability analysis since it merely focuses on the parameter identification of *Z*s of MF_b, and thus there is no need to partition MF to use 1-d IRC [4]. One more superiority of the proposed criterion is that the loop IM of MF_b is not sensitive to the initial phase of ideal voltage source, and the basic idea can be extended to any other transfer-function based stability analysis as long a proper MF is selected.

B. Validations

The stability assessments of case 1 are illustrated in Fig. 6. It can be observed that the magnitude of each MF_b owns a pair of nadirs that are symmetrical about the central frequency (0 Hz for the sequence domain, 50 Hz for the *dq* domain, and the peaks/nadirs at ±50 Hz in Fig. 6 (b) and 6 (c) due to the calculation error of difference method are neglected). Consequently, it is more credible that using various MF_bs can achieve the same stability analysis result compared with the inconsistent feature of trajectories using IRCs in Fig. 4 (a) and 4 (c), which is an advantage of the proposed criterion.

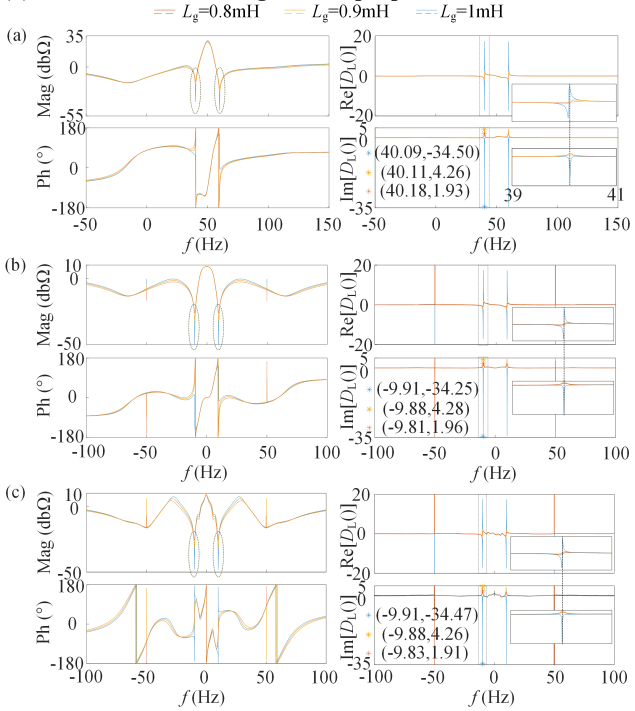

Fig. 6. Impedance characteristics with Re-Im parts of $D_L(MF_b)$. (a) *p*. (b) *d*. (c) *q*.

The logarithmic derivatives and Re-Im separations are then performed on each MF_bs to check the stability. It is found that the aforementioned nadirs lead to the zero-crossing points of Re[$D_L(MF_b)$] with definite positive slopes when L_g varies, and a *Z* of each MF_b exists over the certain frequency range. Minimums when L_g=1mH and maximums when L_g=0.9&0.8mH both for Im[$D_L(MF_b)$] are observed, and the extremes are very close in both domains, thus the system is judged as unstable only when L_g=1mH no matter which MF_b is selected. In addition, α_Z is estimated as 0.1821, –1.4749, and –3.2555 when dividing each extreme value by 2π (the x-axis represents *f* instead of ω in Fig. 6) in the sequence domain, and the results match the theoretical calculation in Table III and the simulated divergence rate of u_{dc} in Fig. 3. In a word, the mode is estimated accurately enough to judge the system unstable using the proposed criterion.

V. Conclusion

To deepen the understanding of a typical transfer function-based small-signal stability assessment, the well-known IRCs are comparatively studied using two cases in both *dq* and the sequence domain for converter-based AC systems. It is confirmed that the SISO analysis is successful as long as a proper MF is selected, which is proved by detailed *Z-P* calculations, and thus the MIMO analyses can be fully avoided. The source-load partition introduces uncertainties to the open-loop *P*s even if the subsystems can operate stably when powered by ideal sources, and to avoid such influences on the stability assessment, the system modes implied by the closed-loop characteristic polynomial are especially focused. A novel loop IM-based criterion is proposed aided by the logarithmic derivative of MF frequency responses, which can identify the unstable mode successfully. Such ideas can be extended to the stability analysis of the multi-terminal AC/DC, the unbalanced AC, and the harmonically distorted AC systems in the future.

References

[1] M. Belkhayat, “Stability criteria for AC power systems with regulated loads,” Ph.D. dissertation, Purdue University, Washington, DC, 1997.
[2] J. Sun, “Impedance-based stability criterion for grid-connected inverters,” *IEEE Trans. Power Electron.*, vol. 26, no. 11, pp. 3075–3078, Nov. 2011.
[3] Technical Specification for Assessment of Impedance Characteristics of Wind Farm, NB/T 10651—2021, 2021.
[4] C. Zhang, X. Cai, A. Rygg, and M. Molinas, "Sequence domain SISO equivalent models of a grid-tied voltage source converter system for small-signal stability analysis," *IEEE Trans. Energy Convers.*, vol. 33, no. 2, pp. 741–749, Jun. 2018.
[5] Y. Gu and T. C. Green, “Power system stability with a high penetration of inverter-based resources,” *Proc. IEEE.*, early access, doi: 10.1109/JPROC.2022.3179826.
[6] H. Liu, X. Xie, and W. Liu, “An oscillatory stability criterion based on the unified dq-frame impedance network model for power systems with high-penetration renewables,” *IEEE Trans. Power Syst.*, vol. 33, no. 3, pp. 3472–3485, May 2018.
[7] D. Yang and X. Wang, “Unified modular state-space modeling of grid-connected voltage-source converters,” *IEEE Trans. Power Electron.*, vol. 35, no. 9, pp. 9700–9715, Sep. 2020.